

# Effect of corner modifications on 'Y' plan shaped tall building under wind load

Prasenjit Sanyal<sup>1a</sup> and Sujit Kumar Dalui<sup>\*2</sup>

<sup>1</sup>Department of Civil Engineering, Meghnad Saha Institute of Technology, Kolkata-700150, India.

<sup>2</sup>Department of Civil Engineering, Indian Institute of Engineering Science and Technology, Shibpur, Howrah-711103, India

(Received February 28, 2019, Revised September 26, 2019, Accepted February 11, 2020)

**Abstract.** Wind load and responses are the major factors which govern the design norms of tall buildings. Corner modification is one of the most commonly used minor shape modification measure which significantly reduces the wind load and responses. This study presents a comparison of wind load and pressure distribution on different corner modified (chamfered and rounded) Y plan shaped buildings. The numerical study is done by ANSYS CFX. Two turbulence models, k-epsilon and Shear Stress Transport (SST), are used in the simulation of the building and the data are compared with the previous experimental results in a similar flow condition. The variation of the flow patterns, distribution of pressure over the surfaces, force and moment coefficients are evaluated and the results are represented graphically to understand the extent of nonconformities due to corner modifications. Rounded corner shape is proving out to be more efficient in comparing to chamfered corner for wind load reduction. The maximum reduction in the maximum force and moment coefficient is about 21.1% and 19.2% for 50% rounded corner cut.

**Keywords:** computational fluid dynamics; corner modifications; force coefficient and moment coefficient

## 1. Introduction

With the continuous developments in design methods and construction technologies and in the context of huge urban growth, buildings are becoming more flexible, slender and taller day by day and it poses new design challenges for structural engineers. In addition, there is a need to make the building lighter in order to control the development of inertial forces due to earthquake. This further increases the wind induced forces and motion in a building. Thus, wind induced loads and motions generally governs the design of a tall building. This load and response directly depend on the outer shape of the building model and it can be significantly reduced by some outer shape modifications (Shiraishi *et al.* 1986, Amano 1995, Kawai 1998, Cooper *et al.* 1997, Kim and You 2002, Kim *et al.* 2008, Kim and Kanda 2010a, 2010b, Bairagi and Dalui 2018).

The Y plan shaped building is a triaxial building with three separate wings connected to a central core. Y shape plan is very common for residential, corporate and hotel buildings as it allows the maximum views outward without overlooking a neighboring unit. This type of building is also recommended keeping in view of its ventilation efficiency and faster constructability. The current tallest structure, the Burj Khalifa, and the soon to be the tallest tower, Jeddah

Tower, both are shape modified Y plan shaped tall building (Baker *et al.* 2007).

For a regular rectangular plan shaped building model, windward face generally experiences critical pressure distribution, but irregular or unconventional plan shaped buildings sometimes experience critical pressure distribution

on other faces also. Responses to unconventional plan shaped buildings due to wind are estimated by employing wind tunnel techniques or numerically by computational fluid dynamics. Researchers in the field of wind engineering conducted some works on unconventional plan shape high rise buildings. Gomes *et al.* (2005) experimentally and analytically studied wind pressure on different faces of 'U' and 'L' plan shaped tall buildings. Wind pressure distribution on various facets of these building models were observed to be different from that of a square model. Irwin (2009) explains new wind engineering challenges of buildings higher than 300 m. He discussed the force balance technique, aeroelastic modeling, high frequency pressure integration tests, as well as the traditional pressure model and pedestrian wind studies of super tall buildings. Experimental investigation of the aerodynamic characteristics of various triangular shaped tall buildings was done by Kumar *et al.* (2013). Raj and Ahuja (2013) compared the base shear, base moment and twisting moment of three rigid building models having the same floor area, but different cross-sectional shapes by changing the wind incidence angle. Muehleisen and Patrizi (2013) compared a huge set of data and derived a parametric equation of pressure coefficient. Bandi *et al.* (2013) investigated the aerodynamic characteristics of different triangular plan shaped tall buildings with aerodynamic

\*Corresponding author, Assistant Professor  
E-mail: [sujit\\_dalui@rediffmail.com](mailto:sujit_dalui@rediffmail.com)

<sup>a</sup>Assistant Professor, Ph.D. Student  
E-mail: [prasenjitsanyal14@gmail.com](mailto:prasenjitsanyal14@gmail.com)

modifications using a wind tunnel test. Experimental and analytical results for wind pressure distribution on various facets of 'Y' shape tall buildings were presented by Mukherjee *et al.* (2014). Peculiar pressure distribution has been observed on certain faces due to self-interference effect. Chakraborty *et al.* (2014) presented a numerical and experimental study of '+' plan shaped tall building for 0° and 45° wind angle. Yi and Li (2015) made a full-scale as well as a wind tunnel study on a super tall building situated in Hong Kong. To measure force, high-frequency force balance technique and to measure pressure coefficient synchronize multi-pressure sensors are used respectively in a wind tunnel. The responses from wind tunnel were seen to be quite comparable with full-scale results. The inter-building and intra-building aerodynamic behaviors of linked buildings were investigated by Song *et al.* (2016). Wind effect of internal angles between limbs of cross plan shaped tall building was studied by Kumar and Dalui (2016). Li and Li (2016) conducted a wind tunnel test to compute wind effects on "L" plan shaped tall building under dynamic across wind. They proposed an empirical formula to quantify across-wind dynamic load on "L" plan shaped tall building by taking side ratio and terrain category as the variable. Such empirical formula can help a practicing engineer to quantify wind load directly without rigorous calculation. Sanyal and Dalui (2018) investigated the aerodynamic effects of the opening of a rectangular building in the presence of the courtyard. Bhattacharya and Dalui (2018) presented analytical and experimental results of pressure distribution on various facets of 'E' plan shape tall buildings for various wind incidence angles. They also proposed polynomial expressions for obtaining mean wind pressure coefficient on all the faces of the building model by using the Fourier series expansion.

The concept of corner modification is very common for automotive system (Watkins and Vano 2008, Cheng *et al.* 2011, Abdul Ghani *et al.* 2001, Modi *et al.* 1995, Kassim and Filippone 2010, Jacobsen 2006, Watkins *et al.* 1993, Gillieron and Chometon 2001). Engineers are now also applying the concept of corner modifications in different high-rise buildings. Researchers have conducted some great works on aerodynamic load reduction of tall buildings by corner modifications.

Kwok and Bailey (1987) and Kwok *et al.* (1988) have done experimental study and investigated the effects of fins, vented fins and slotted corner on square shape tall building. They found that Fins and slotted fins increase the along-wind responses and reduce the response on across-wind direction. They also commented that slotted corners reduce both along- and across-wind responses. Kawai (1998) has done wind tunnel test of square and rectangular sections with rounded, chamfered and recessed corners. He commented that small chamfers and recessions are effective in preventing aeroelastic instability. While rounded corners increase the aerodynamic damping. Miyashita *et al.* (1993) explained the characteristics of the wind forces acting on X and Y axis and presented the detailed responses on a square building with chamfered corners or openings. Tamura *et al.* (1998) used CFD as the tool to find out the aerodynamic improvement of square section by corner modifications.

Tamura and Miyagi (1999) calculated the decrease in drag force of square sections with rounded and chamfered corners using wind tunnel. Gu and Guan (2004) did wind tunnel experiments on Square and rectangular sections with chamfered and recessed corners. The effects of terrain category, aspect ratio and side ratio are investigated for different cross-sections. The formulas for the power spectra of the across-wind dynamic forces, the coefficients of base moment and shear force are derived. Zhengwei *et al.* (2012) investigated 14 square tall buildings models with recessed corners in two differently simulated wind fields to observe the aerodynamic consequences.

Tanaka *et al.* (2012) done wind tunnel experiments on square sections with recessed and chamfered corners and also used other global modifications such as twisting, openings, tapering and set-backs. They also reported base moments and moment coefficients of various configurations. Elshaer *et al.* (2014) done CFD analysis of square section with rounded, chamfered and recessed corners using 2D flow and different inflow velocities. They concluded that round corners are effective in reducing drag followed by chamfered and then recessed shapes. Elshaer *et al.* (2014), Elshaer *et al.* (2015), and Elshaer *et al.* (2017) presented detailed analytical study on wind performance enhancement of tall buildings using twisting and corner aerodynamic optimization. They have used Large eddy simulation (LES) models for numerical simulation of the wind behavior, and utilized genetic algorithm (GA) for the optimization process.

In the present study, effects of corner modifications on "Y" plan shaped tall building are studied numerically by Computational Fluid Dynamics (CFD) technique. More specifically, force coefficient, moment coefficient and local wind pressure variation of the corner modified "Y" plan shaped tall buildings are studied for 0°, 30° and 60° angle of attack. In order to validate the results, found from the numerical study, the results are compared with previous wind tunnel test data.

Grid sensitivity test and dependency of the air velocity on aerodynamic coefficients are also studied.

Along with this, streamlines around the building models are studied using CFD. Local pressure distribution on different faces of the building models are thoroughly examined to understand the complex wind phenomena occurring due to the corner shape modifications.

## 2. Scope of work

The buildings are modeled in 1:300 length scale. Model A with sharp corner is shown in Fig. 1. The two types of corner modifications are shown in Figs. 2 and 3 consist of Model B (chamfered corner) and Model C (Rounded corner) developing from the fundamental Model A. The isometric view and different faces of the Model A is shown in Figs. 4 and 5 respectively. The corner regions of the chamfered and rounded building model are shown in Figs. 6 and 7.

The corner cut ratio is defined as  $\gamma_c = b/B = d/D$ . Where 'B' and 'D' denotes width and breadth of the Y section, and

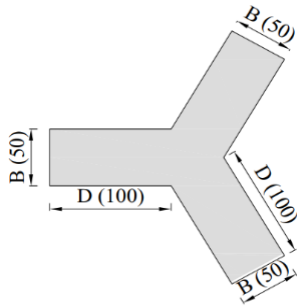


Fig. 1 Model A (Sharp)

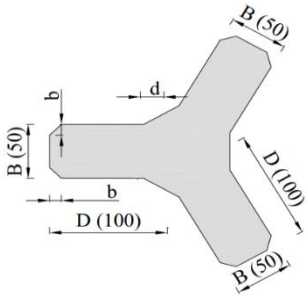


Fig. 2 Model B (Chamfered)

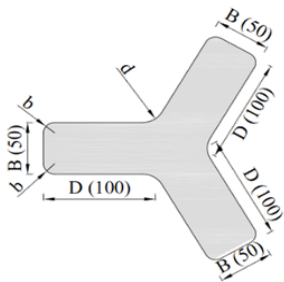


Fig. 3 Model C (Rounded)

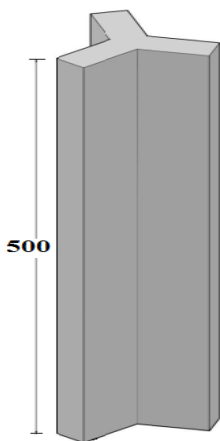


Fig. 4 Isometric view of Model A (in mm)

for the present work these are taken as 50 mm and 100 mm. 'b' is the cutting length of corner C1, C3, C4, C6, C7, C9 and 'd' are the cutting length of corner C2, C5, C8. By varying the amount of  $\gamma_c$ , the effects of corner modification on Y plan shaped tall building have been studied. The models used to comprehend the wind-induced behavior is shown in Table 1.

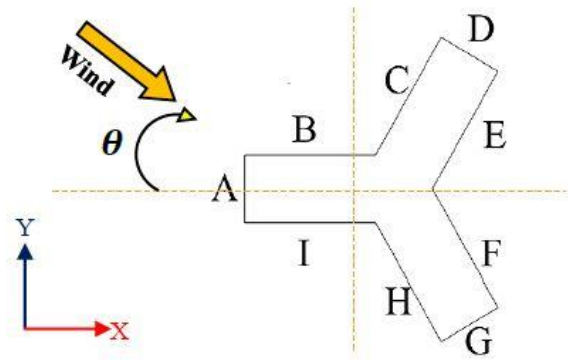


Fig. 5 Wind incidence angle ( $\theta$ ) with respect to plan ( $0^\circ \leq \theta \leq 60^\circ$ )

Table 1 Testing cases types

Corner modified model	Corner cut ratio $\gamma_c = b/B = d/D$	Wind angle	Mean wind speed at reference height (m/s)
Model B	0%, 10%, 20%, 30%	$0^\circ, 30^\circ, 60^\circ$	10
Model C	0%, 10%, 20%, 30%, 40%, 50%	$0^\circ, 30^\circ, 60^\circ$	10

### 3. Numerical analysis of the tall building by ANSYS CFX

The boundary conditions used in the numerical simulation are similar to the boundary condition used by Mukherjee *et al.* (2014).

The boundary layer wind profile is governed by the power law equation

$$U(z) = U_0(Z/Z_0)^\alpha \quad (1)$$

Where  $U(z)$  is velocity at some particular height  $Z$ .  $U_0$  is boundary Layer Velocity,  $Z_0$  is the boundary layer depth,  $\alpha$  is the power law exponent and its value is taken as 0.133 which satisfies the open terrain with well scattered obstruction as found by Mukherjee *et al.* (2014).

#### 3.1 Domain and meshing

A domain having 5H, 15H, 5H and 5H inlet, outlet, two side aspect and top clearances from the borders of the building, where H is the height of the model as shown in Fig. 8. The length scale is taken as 1:300. This domain is constructed as per the recommendation of Franke *et al.* (2004). Such a large domain is good enough to avoid the influence of these boundaries on the developed wind flow. Tetrahedral type meshing is done as per the guidelines of Chakraborty *et al.* (2014), (Fig. 9). The mesh near the building is made finer compared to other location for accurately checking the wind parameters. The mesh inflation is provided near the boundaries to provide a smooth flow. The boundary layer wind velocity is taken as 10 m/s. No slip wall is considered at building faces and the bottom. Free slip wall is considered for the top and side faces of the domain. The relative pressure at the outlet is

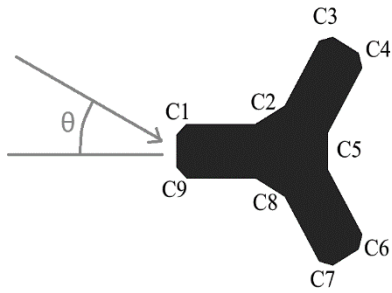


Fig. 6 Corners regions of model B

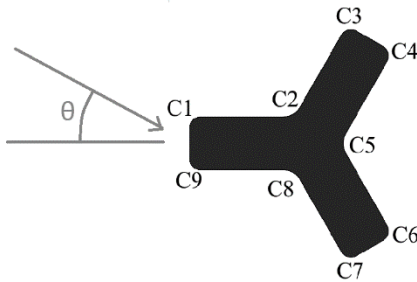


Fig. 7 Corners regions of model C

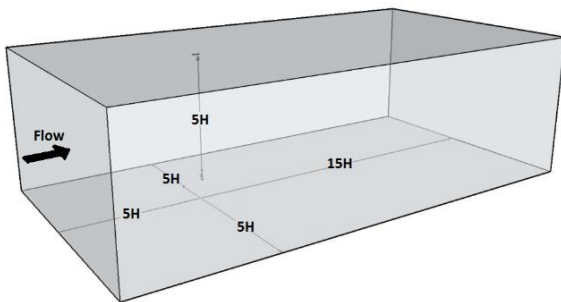


Fig. 8 Domain used for CFD simulation

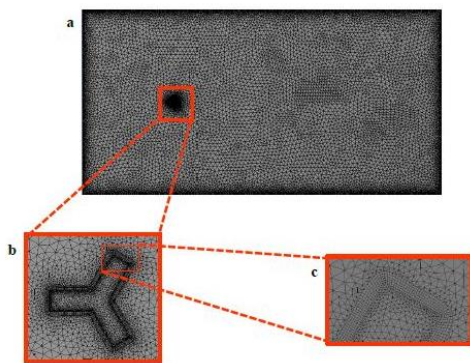


Fig.9 (a) Typical mesh pattern in the computational domain (b) Meshing around the building model (c) Detail of mesh near edge

taken as 0 Pa. The operating pressure in the domain is 1atm, i.e., 101,325 Pa.

### 3.2 Validation

Before starting the numerical analysis of the different model, the results from ANSYS CFX package need to be

validated. For this reason, Model A is analyzed in the aforementioned domain by K- $\epsilon$  and SST turbulence model for  $0^\circ$  and  $60^\circ$  wind incidence angle using ANSYS CFX. The free stream velocity is taken as 10 m/s at the inlet. The domain is constructed as per the recommendation of Franke *et al.* (2004) as mentioned earlier. The velocity profile and turbulence intensity profile along the height of the domain are plotted in the Figs. 10 (a) and 10(b) and compared with the previous experimental data of Dalui (2008) and Mukherjee *et al.* (2014) in similar kind of wind environment.

The face average values of pressure coefficient are determined and compared with the experimental results of Mukherjee *et al.* (2014).

The external pressure coefficient ' $C_p$ ' is calculated using the formula

$$C_p = P / 0.5\rho U_H^2 \quad (2)$$

where  $P$  is the actual wind pressure,  $\rho$  is the density of air and  $U_H$  is the reference velocity at the building height. The external pressure coefficients,  $C_p$  (face average value), for the different faces of the model are listed and compared with experimental results as shown in Fig.11 and Fig.12.

For better understanding between two turbulence model and experimental results the pressure coefficients along the horizontal centerlines around the building periphery for  $0^\circ$  and  $60^\circ$  wind incidence angle are compared.

From Figs. 11 and 12 it can be seen that the results found by both turbulence models are approximately the same as the values obtained experimentally by Mukherjee *et al.* (2014). And from Figs. 13 and 14 it is observed that the horizontal centerlines obtained from the k- $\epsilon$  model have a better agreement with the experimental results compared to those from the SST model. Mukherjee *et al.* (2014) have also concluded that the SST models can predict responses more accurately in the high turbulence zone while the k- $\epsilon$  model is better for overall moderate turbulence.

RANS (Reynolds-averaged Navier - Stokes) simulation is generally said to be less effective for flows with large separation and wake regions, but for our current computational setup it is find out that the results near the separation zones are highly comparable with the wind tunnel results and the computation cost is also very reasonable.

The further analysis has been done based on the k- $\epsilon$  turbulence model.

### 3.3 Details of the turbulence model

k- $\epsilon$  turbulence model is used for the numerical simulation. The k- $\epsilon$  model uses the gradient diffusion hypothesis to relate Reynolds stresses to mean velocity gradients and turbulent viscosity. Turbulent viscosity is modeled as the product of turbulent length scale and turbulent velocity.  $k$  is the turbulent kinetic energy and is defined as the variability of fluctuations in velocity. It has dimensions of  $L^2 T^{-2}$ .  $\epsilon$  is the turbulence eddy dissipation which is actually the rate at which the velocity fluctuation dissipates and has dimensions of per unit time.

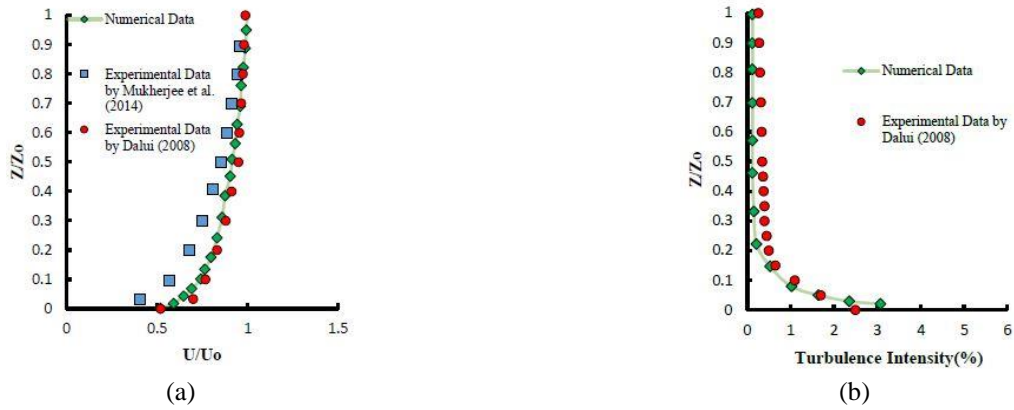


Fig. 10 (a) Variation of velocity with height near the model and (b) variation of turbulence intensity with the height near the model

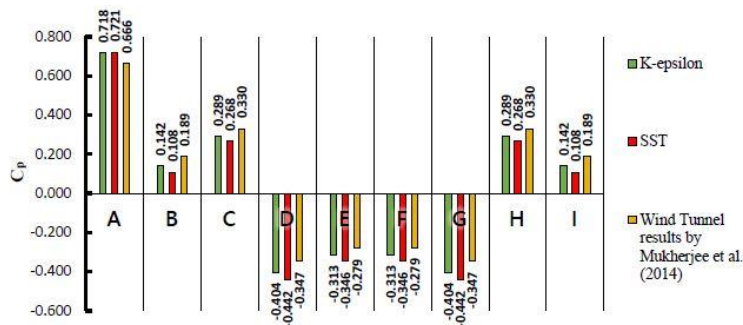


Fig. 11 Comparison of mean pressure coefficients on different surfaces of model A between numerical results and experimental result by Mukherjee *et al.* (2014) for 0° wind incidence angle

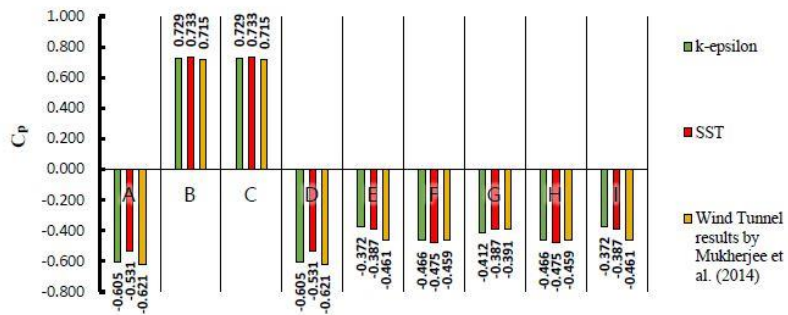


Fig. 12 Comparison of mean pressure coefficients on different surfaces of model A between numerical results and experimental result by Mukherjee *et al.* (2014) for 60° wind incidence angle

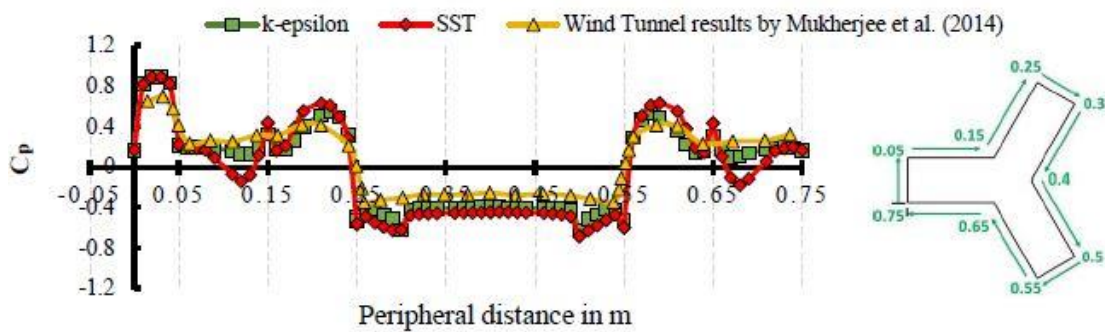


Fig. 13 Comparison of pressure coefficients around the building (model A) at mid-depth for k-ε model, SST model and experimental results by Mukherjee *et al.* (2014) for 0° wind incidence angle

The continuity and momentum equations are

$$\frac{\partial \rho}{\partial t} + \frac{\partial(\rho U_j)}{\partial x_j} = 0 \quad (3)$$

$$\frac{\partial \rho U_i}{\partial t} + \frac{\partial(\rho U_i U_j)}{\partial x_j} = -\frac{\partial P'}{\partial x_i} + \frac{\partial}{\partial x_j} \left[ \mu_{eff} \left( \frac{\partial U_i}{\partial x_j} + \frac{\partial U_j}{\partial x_i} \right) \right] + S_M \quad (4)$$

where  $S_M$  is the sum of body forces,  $\mu_{eff}$  is the effective viscosity accounted for turbulence, and  $P'$  is the modified pressure. Density and velocity are denoted by  $\rho$  and  $U$ .

The k- $\epsilon$  model is based on the concept of eddy viscosity, so that

$$\mu_{eff} = \mu + \mu_t \quad (5)$$

Where  $\mu_t$  is turbulent viscosity

$$\mu_t = C_\mu \rho \frac{k^2}{\epsilon} \quad (6)$$

The values of  $k$  and  $\epsilon$  come from the differential transport equations of turbulence kinetic energy and turbulence dissipation rate

$$\begin{aligned} & \frac{\partial(\rho k)}{\partial t} + \frac{\partial(\rho k U_j)}{\partial x_j} \\ &= \frac{\partial}{\partial x_j} \left[ \left( \mu + \frac{\mu_t}{\sigma_k} \right) \frac{\partial k}{\partial x_j} \right] + P_k + P_b - \rho \epsilon - Y_M + S_k \end{aligned} \quad (7)$$

$$\begin{aligned} & \frac{\partial(\rho \epsilon)}{\partial t} + \frac{\partial(\rho \epsilon U_j)}{\partial x_j} = \frac{\partial}{\partial x_j} \left[ \left( \mu + \frac{\mu_t}{\sigma_\epsilon} \right) \frac{\partial \epsilon}{\partial x_j} \right] + \rho C_1 S_\epsilon \\ & - \rho C_2 \frac{\epsilon^2}{k + \sqrt{\nu \epsilon}} + C_{1\epsilon} \frac{\epsilon}{k} C_{3\epsilon} P_b + S_\epsilon \end{aligned} \quad (8)$$

$P_k$  represents the generation of turbulence kinetic energy due to the mean velocity gradients,  $P_b$  represents the generation due to buoyancy and  $Y_m$  represents the contribution of fluctuating dilatation incompressible turbulence to overall dissipation rate,  $C_1$  and  $C_2$  are constants.  $\sigma_k$  and  $\sigma_\epsilon$  are the turbulent Prandtl numbers for  $k$  (turbulence kinetic energy) and  $\epsilon$  (dissipation rate). The values considered for  $C_{1\epsilon}$ ,  $\sigma_k$  and  $\sigma_\epsilon$  are taken as 1.44, 1 and 1.3 respectively as per the recommendation of Jones and Launder (1972).

### 3.4 Grid-sensitivity analysis

In this study, a grid-sensitivity analysis (Derakhshandeh and Alam, 2018) is carried out for reducing the discretization errors and the total computational time. The analysis is performed for four grids namely MC1, MC2, MC3 and MC4. The method of Grid Convergence Index (GCI) as recommended by Celik *et al.* (2008) was utilized to find out that the selected grid resolution is sufficient or not to precisely capture the wind characteristics.

The Force coefficient ( $C_F$ ) and Moment coefficient ( $C_M$ ) calculated using equations 9-14 are shown and compared in Table-2 for the four grids. The results reveal that  $C_F$  and  $C_M$  converge for mesh case 3 (MC3), with a percentage of error of 0.93% and 0.32% respectively. Hence, for the rest of the simulation, MC3 is chosen. The detailed mesh pattern shown in Fig. 9 is actually of MC3 case.

Table 2 Typical mesh refinement test for sharp edged Y plan shaped building

Mesh case	Mesh Quality	No of cell	$C_F$	% Error	$C_M$	% Error
MC1	Very coarse	2037707	0.751	3.74%	0.825	1.56%
MC2	Coarse	4368988	0.745	2.81%	0.816	0.51%
MC3	Refined	7930277	0.731	0.93%	0.815	0.32%
MC4	Very refined	15119834	0.724	-	0.812	-

## 4. Results

### 4.1 Flow pattern

The velocity field around the models for various wind angles, as obtained from the k- $\epsilon$  method is shown in Fig 15. The wind separates away at the edges of the windward face and reverts back after that. This results in high wind velocity at the corner region of the windward side. For chamfered and rounded corner shapes, velocity at this corner region is much higher than the sharp corner. Rounded shape experiences maximum velocity at this corner region and this also increases with  $\gamma_c$ . This higher velocity and direct side wash will produce huge negative pressure at these corner portions.

For  $0^\circ$  and  $60^\circ$  wind angle, the vortices formed in the wake region are almost symmetrical. This will create an identical distribution of pressure on the symmetrical faces. For model A the sizes of the eddies are more. With the increase in the corner cut the eddy size decreases. As the eddy size is minimum for Model C (Rounded) it will experience the lesser wind force compared to Model A and Model B. Velocity fields around Model C ( $\gamma_c=30\%$ ) for  $0^\circ$ ,  $120^\circ$  and  $240^\circ$  angle of attack are shown in Fig. 16. For  $0^\circ$  wind angle maximum velocity occurs near corner C3 and C7. And as the building is triaxially symmetrical, the same phenomena occur near corner C1 and C6 for  $120^\circ$  angle of attack and near C4 and C9 for  $240^\circ$  angle of attack. So, the corners of the shorter edges are more vulnerable to wind attack.

### 4.2 Pressure distribution

The pressure contour of different faces along with flow lines around Model A, B and C for  $0^\circ$  wind angle is shown Fig. 17. Symmetrical faces are having identical pressure distribution due to the symmetry in the flow pattern. As expected, the positive pressure distribution has been observed on Face A with maximum pressure at the stagnation point. The pressure decreases as we move toward the edges. Pressure distribution is parabolic in nature due to boundary layer flow and symmetrical about the vertical centerline. Other portions of the different models also encounter a similar kind of pressure distribution. The main difference in pressure for the three models occurs in corner C3 and C7 portion for  $0^\circ$  angle of attack. For Model C huge negative pressure generates in these portions. This mainly happens due to side-wash of these corner faces.

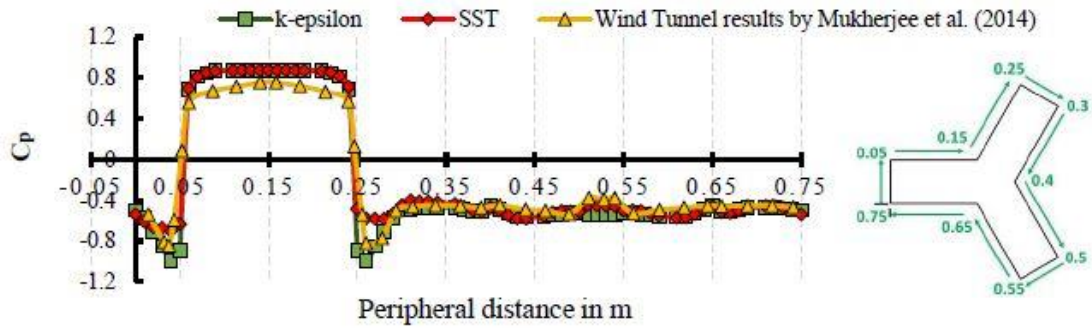


Fig. 14 Comparison of pressure coefficients around the building (model A) at mid-depth for k- $\epsilon$  model, SST model and experimental results by Mukherjee *et al.* (2014) for 60° wind incidence angle

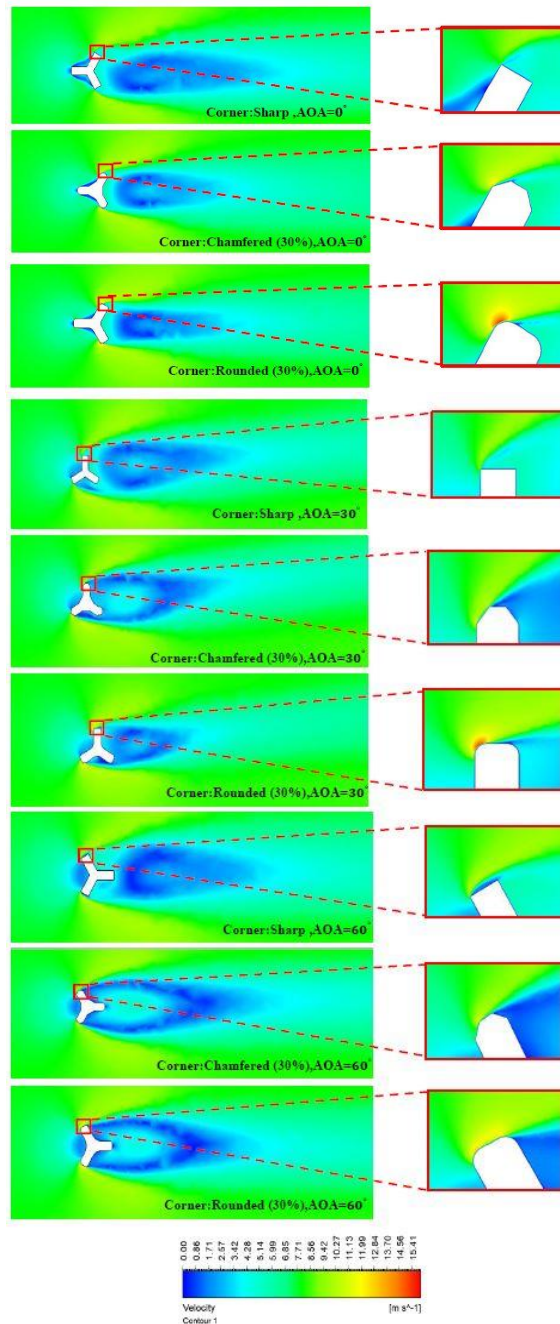


Fig. 15 Velocity field for different corner shapes

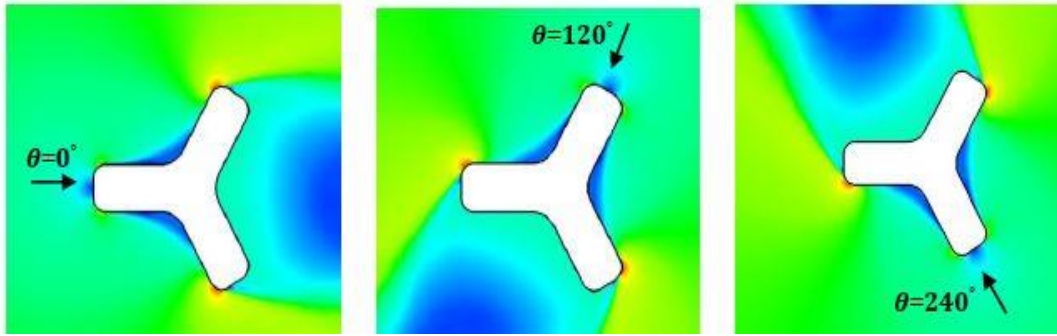


Fig. 16 Velocity flow around model C ( $\gamma_c=30\%$ ) for  $0^\circ$ ,  $120^\circ$  and  $240^\circ$  angle of attack (Velocity contour is same as Fig. 15)

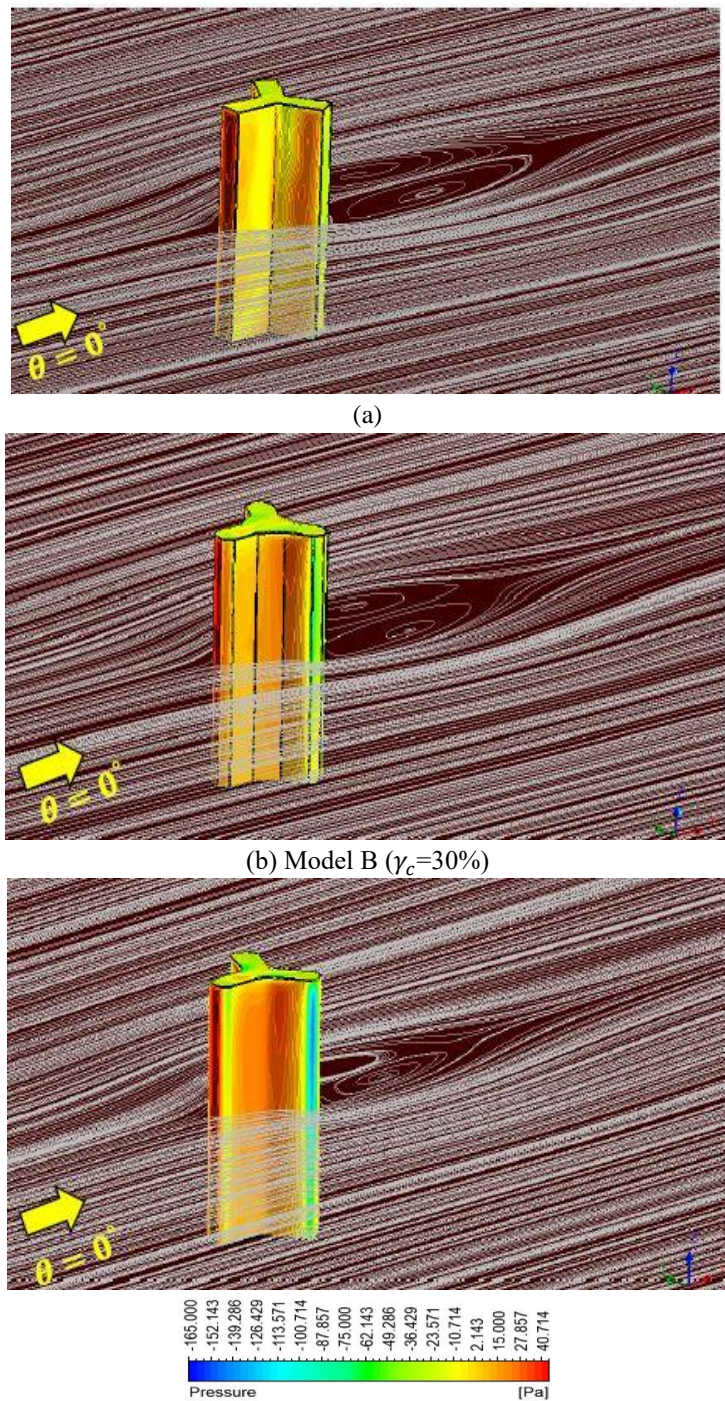


Fig. 17 Pressure contours and streamlines of various models for  $0^\circ$  wind angle

Table 3 Variation of force Coefficient with various wind incidence angle for model B

$\gamma_c$ (%)	AOA=0°		AOA=30°		AOA=60°	
	$C_{Fx}$	$C_{Fy}$	$C_{Fx}$	$C_{Fy}$	$C_{Fx}$	$C_{Fy}$
0	0.731	-0.016	0.451	-0.972	0.335	-0.877
10	0.659	-0.019	0.408	-0.938	0.375	-0.766
20	0.638	0.011	0.338	-0.961	0.374	-0.782
30	0.604	-0.015	0.279	-0.959	0.404	-0.771

Table 4 Variation of force coefficient with various wind incidence angle for model C

$\gamma_c$ (%)	AOA=0°		AOA=30°		AOA=60°	
	$C_{Fx}$	$C_{Fy}$	$C_{Fx}$	$C_{Fy}$	$C_{Fx}$	$C_{Fy}$
0	0.731	-0.016	0.451	-0.972	0.335	-0.877
10	0.686	0.020	0.429	-0.863	0.312	-0.752
20	0.595	-0.012	0.280	-0.906	0.356	-0.679
30	0.530	-0.016	0.201	-0.874	0.353	-0.639
40	0.506	0.000	0.198	-0.875	0.333	-0.631
50	0.422	-0.001	0.169	-0.828	0.305	-0.572

Table 5 Variation of moment coefficient with various wind incidence angle for model B (Chamfered model)

$\gamma_c$ (%)	AOA=0°		AOA=30°		AOA=60°	
	$C_{Mx}$	$C_{My}$	$C_{Mx}$	$C_{My}$	$C_{Mx}$	$C_{My}$
0	-0.008	0.815	-0.989	0.589	-0.935	0.403
10	-0.015	0.757	-0.968	0.518	-0.800	0.387
20	0.012	0.713	-1.011	0.390	-0.807	0.392
30	-0.010	0.697	-1.014	0.339	-0.807	0.427

Table 6 Variation of moment coefficient with various wind incidence angle for model C (rounded model)

$\gamma_c$ (%)	AOA=0°		AOA=30°		AOA=60°	
	$C_{Mx}$	$C_{My}$	$C_{Mx}$	$C_{My}$	$C_{Mx}$	$C_{My}$
0	-0.008	0.815	-0.989	0.589	-0.935	0.403
10	0.012	0.790	-0.910	0.540	-0.828	0.377
20	-0.017	0.673	-0.967	0.346	-0.719	0.372
30	-0.010	0.598	-0.937	0.287	-0.681	0.367
40	0.000	0.574	-0.934	0.286	-0.689	0.351
50	0.002	0.478	-0.902	0.227	-0.639	0.333

### 4.3 Force and moment coefficients

For studying the variation of wind effect for different wind angle, the global force and moment coefficients ( $C_F$  and  $C_M$ ) are defined as follows (Sun *et al.* 2017)

$$C_{Fx} = \frac{F_x}{0.5\rho U_H^2 \cdot A_x} = \frac{\sum_i C_{pi} A_i \cos\alpha_i}{\sum_i A_i \cos\alpha_i} \quad (9)$$

$$C_{Fy} = \frac{F_y}{0.5\rho U_H^2 \cdot A_y} = \frac{\sum_i C_{pi} A_i \sin\alpha_i}{\sum_i A_i \sin\alpha_i} \quad (10)$$

$$C_F = \sqrt{C_{Fx}^2 + C_{Fy}^2} \quad (11)$$

$C_F$  is the global force coefficient of the whole building;  $C_{Fx}$  and  $C_{Fy}$  are the force coefficients of the whole building along X and Y axis;  $F_x$  and  $F_y$  are the value of

total force exported from ANSYS CFX in the x and y-direction, ' $\rho$ ' is the density of wind,  $U_H$  is the reference velocity at the building height,  $C_{pi}$  is the pressure coefficient of point  $i$ , ' $A_i$ ' is the subsidiary area of point  $i$ ;  $\sin\alpha$  and  $\cos\alpha$  are the direction vector of point  $i$  along X and Y axis.

$$C_{Mx} = \frac{M_x}{0.5\rho U_H^2 \cdot A_y \cdot 0.5L} = \frac{\sum_i C_{pi} A_i z_i \sin\alpha_i}{0.5L \cdot \sum_i A_i \sin\alpha_i} \quad (12)$$

$$C_{My} = \frac{M_y}{0.5\rho U_H^2 \cdot A_x \cdot 0.5L} = \frac{\sum_i C_{pi} A_i z_i \cos\alpha_i}{0.5L \cdot \sum_i A_i \cos\alpha_i} \quad (13)$$

$$C_M = \sqrt{C_{Mx}^2 + C_{My}^2} \quad (14)$$

$C_M$  is the global moment coefficient of the whole building,  $C_{Mx}$ ,  $C_{My}$  are the moment coefficients of the whole building along X and Y axis;  $M_x$  and  $M_y$  are the value of the total moment along the X and Y-direction.  $Z_i$  is the distance from point  $i$  to the moment calculation point;  $L$  is the height of whole building.

$C_{Fx}$ ,  $C_{Fy}$  and  $C_{Mx}$ ,  $C_{My}$  for Model B and C for various wind angles are tabulated in Tables 3 - 6. The graphical representation of Force coefficient ( $C_F$ ) and Moment coefficient ( $C_M$ ) is shown in Fig. 18.

Both force and moment coefficient decrease with increase in  $\gamma_c$ . These decrease in values is comparatively more for Model C (Rounded corner). So, rounded corner is more efficient in wind load reduction in compare to the chamfered corner.

### 4.4 Comparison of $C_p$ along the perimeter of the building models

Graphical plots representing the variation of pressure coefficient along the perimeter of Model B (Chamfered model) at mid height for various angles of attack are shown in Figs. 19 - 21. From the figure it is quite clear that the major increase in the negative pressure occurs in the corner portions (C3 and C7 corner for 0° wind angle) of the building models.

And this effect generally increases with the increase in the corner cut. So, the total exerted force and moment of the building decreases with the increase in corner cut but on the other hand it increases the maximum negative local pressure at the corner regions by a huge amount. So, from the designing point of view, all of these effects must be considered separately.

The variation of pressure coefficient along the perimeter of Model C (Rounded model) at mid height for various angles of attack is shown in Figs. 22 - 24. Like Model B, the huge increase in the negative pressure on the corner portions also happens due to separation of flow and side wash. Though the maximum studied  $\gamma_c$  for Model C is 50% the maximum negative pressures at these corner regions occurs for 40% corner cut. Thus, providing completely rounded corner ( $\gamma_c=50\%$ ) is two way beneficial.

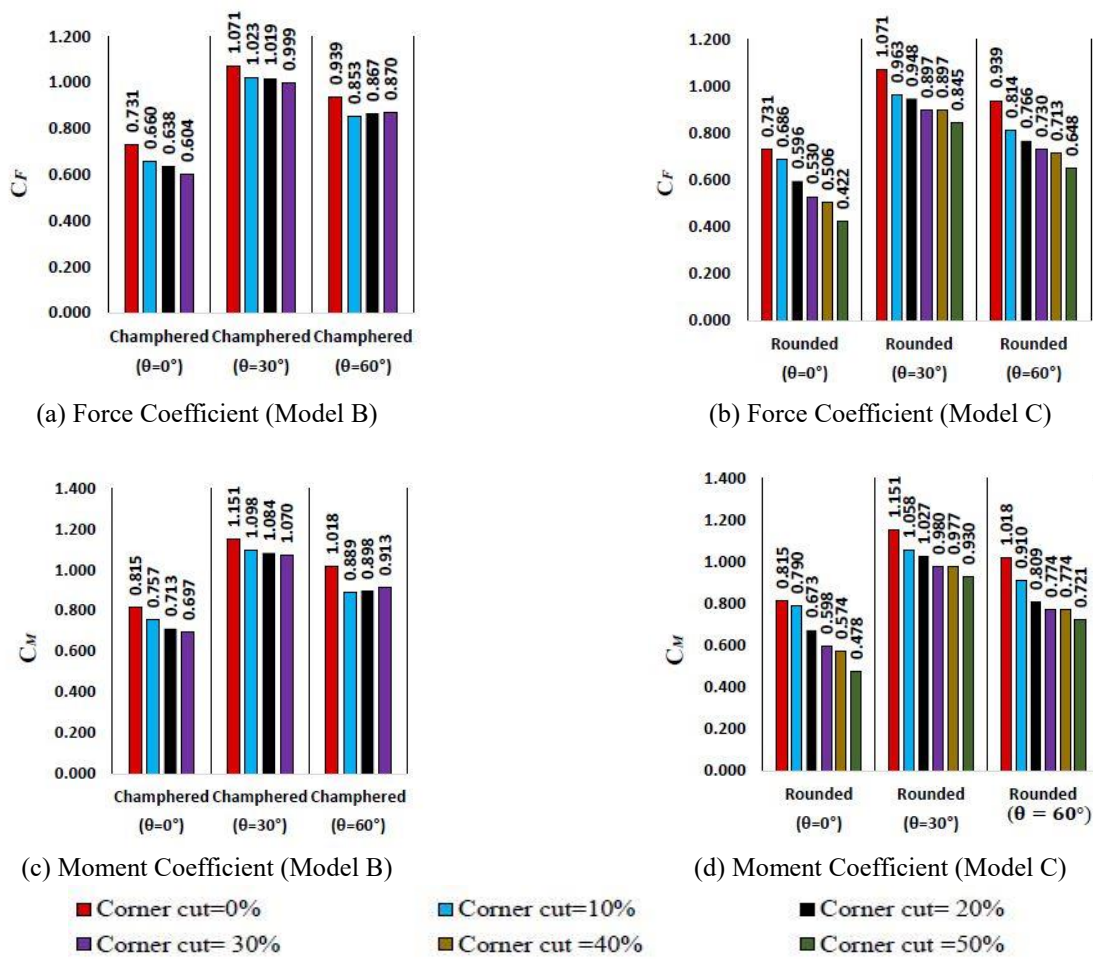


Fig.18 Comparison of force and moment coefficients for various percentage of corner cut

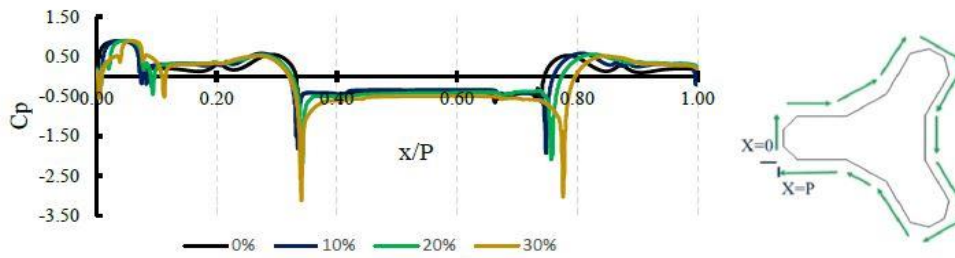


Fig. 19 Variation of pressure coefficients along perimeter of Model B ( $\gamma_c=0\%, 10\%, 20\%, 30\%$ ) at mid height for  $0^\circ$  wind incidence angle

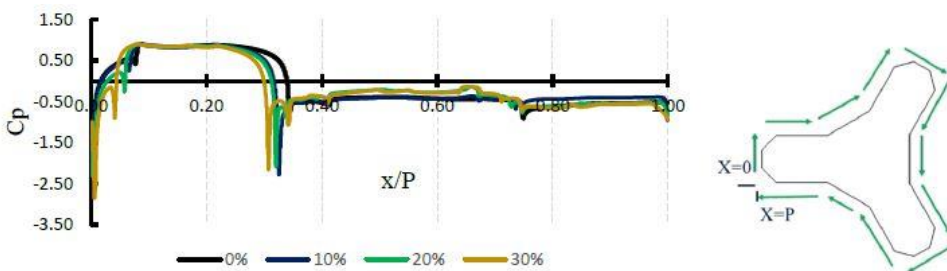


Fig. 20 Variation of pressure coefficients along perimeter of Model B ( $\gamma_c=0\%, 10\%, 20\%, 30\%$ ) at mid height for  $30^\circ$  wind incidence angle

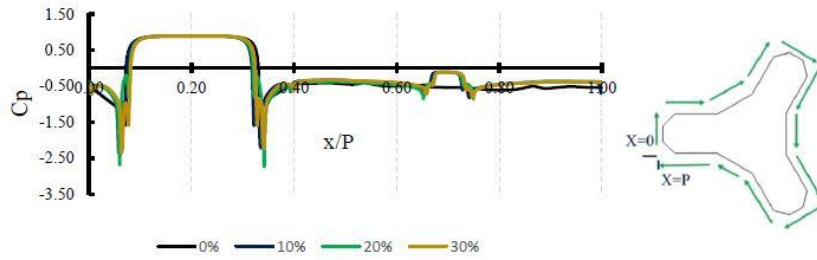


Fig. 21 Variation of pressure coefficients along perimeter of Model B ( $\gamma_c=0\%$ , 10%, 20%, 30%) at mid height for  $60^\circ$  wind incidence angle

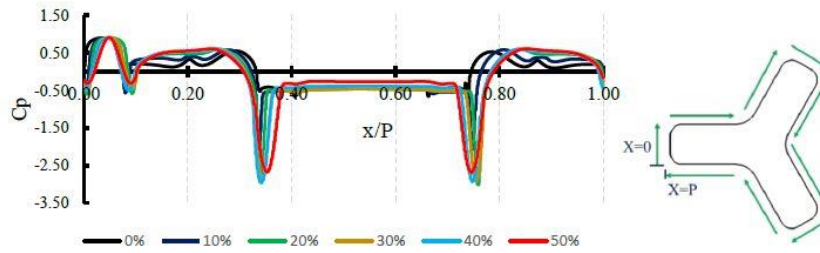


Fig. 22 Variation of pressure coefficients along perimeter of Model C ( $\gamma_c=0\%$ , 10%, 20%, 30%, 40%, 50%) at mid height for  $0^\circ$  wind incidence angle

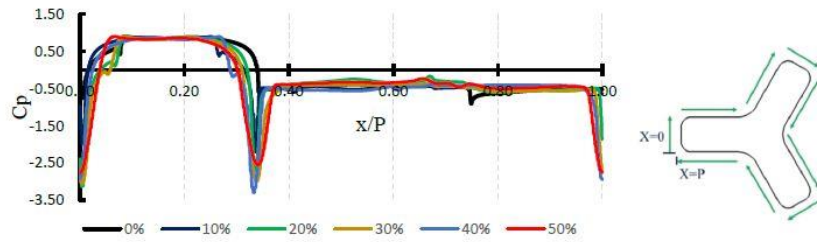


Fig. 23 Variation of pressure coefficients along perimeter of Model C ( $\gamma_c=0\%$ , 10%, 20%, 30%, 40%, 50%) at mid height for  $30^\circ$  wind incidence angle

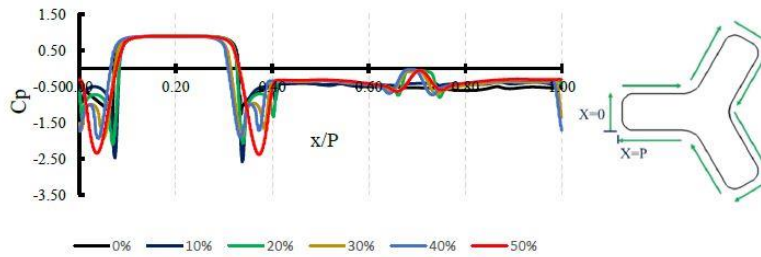


Fig. 24 Variation of pressure coefficients along perimeter of Model C ( $\gamma_c=0\%$ , 10%, 20%, 30%, 40%, 50%) at mid height for  $60^\circ$  wind incidence angle

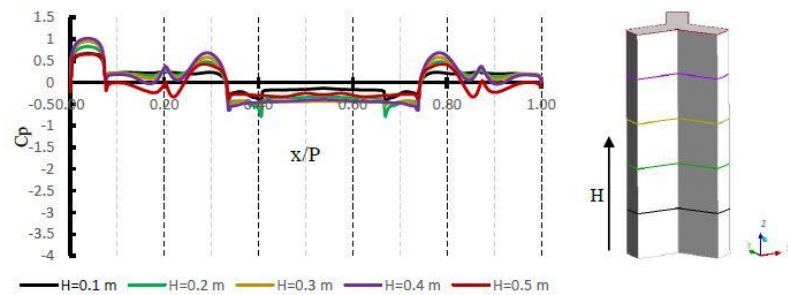


Fig.25 Variation of pressure coefficients along perimeter of Model A at different height for  $0^\circ$  wind incidence angle

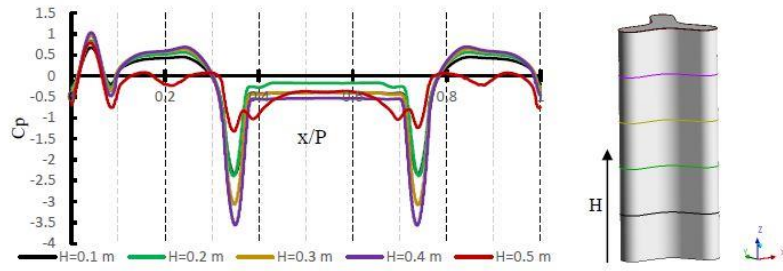


Fig. 26 Variation of pressure coefficients along perimeter of Model C ( $\gamma_c=50\%$ ) at different height for  $0^\circ$  wind incidence angle



Fig. 27 Additional models for analysing the effects of different corner regions

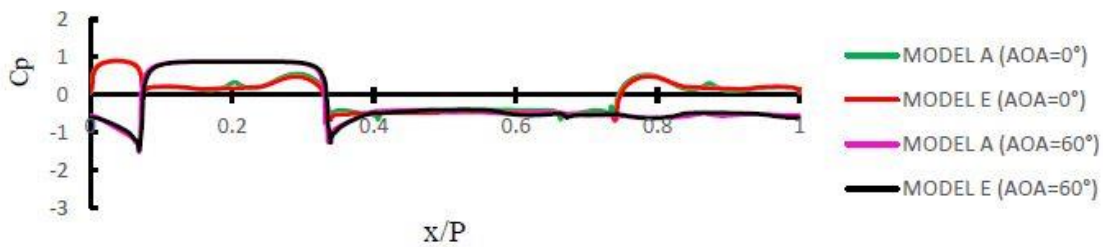


Fig. 28 Variation of pressure coefficients along perimeter of Model A and Model E ( $\gamma_c=50\%$ ) at mid height for  $0^\circ$  and  $60^\circ$  wind incidence angle

Table 7 Comparison of force and moment coefficients of Model A, C, D and E for  $0^\circ$  and  $60^\circ$  angle of attack

	AOA	MODEL A	MODEL C ( $\gamma_c=50\%$ )	MODEL D ( $\gamma_c=50\%$ )	MODEL E ( $\gamma_c=50\%$ )
$C_F$	$\theta = 0^\circ$	0.731	0.422	0.422	0.747
	$\theta = 60^\circ$	0.939	0.648	0.630	0.922
$C_M$	$\theta = 0^\circ$	0.815	0.478	0.485	0.851
	$\theta = 60^\circ$	1.018	0.721	0.723	1.003

Table 8 Comparison of force and moment coefficients of Model A and C ( $\gamma_c = 50\%$ ), for different levels of wind velocity (AOA= $0^\circ$ )

Velocity	Corresponding Reynolds Number	Model A		Model C ( $\gamma_c = 50\%$ )	
		Force coefficient ( $C_F$ )	Moment coefficient ( $C_M$ )	Force coefficient ( $C_F$ )	Moment coefficient ( $C_M$ )
10 m/s	147,707	0.732	0.815	0.422	0.478
20 m/s	295,414	0.739	0.831	0.417	0.481
40 m/s	590,828	0.728	0.819	0.397	0.467

For detail understanding of pressure variation for Model A and Model C ( $\gamma_c=50\%$ ), the local pressure coefficient is

represented graphically in Figs. 25 and 26 along the perimeter at height 0.1 m, 0.2 m, 0.3 m, 0.4 m and 0.5 m. From the comparison of these two graphs it can be concluded that not only these corner regions experience the maximum suction pressure, but these portions also undergo a huge variation in pressure for different heights also.

#### 4.5 Effects of different corner regions

Actually, for both Model B and C we have considered two different types of corner positions. One is on the corner of the shorter edges (C1, C3, C4, C6, C7, and C9) and another is at the junction of the longer edges (C2, C5, and C8). The first type of corners mainly affects the separation of the wind flow. So, for finding out the contributions of the different corner regions we have considered two different models, namely Model D and Model E (Fig. 27). We have compared the values of force and moment coefficient of Model A, Model C ( $\gamma_c=50\%$ ), Model D ( $\gamma_c=50\%$ ) and Model E ( $\gamma_c=50\%$ ) in Table 7. The values of  $C_F$  and  $C_M$  for Model A is almost same with Model E and the coefficients for Model C is almost same with Model D.  $C_p$  along horizontal centerline for these models shown in Figs. 28 and

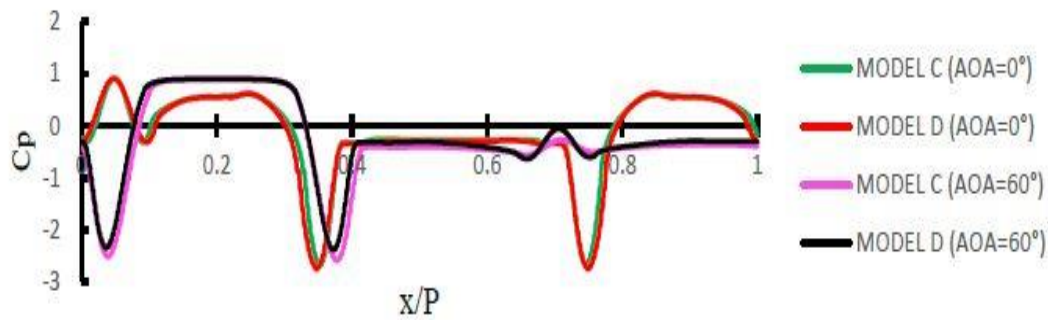


Fig. 29 Variation of pressure coefficients along perimeter of Model C ( $\gamma_c=50\%$ ) and Model D ( $\gamma_c=50\%$ ) at mid height for  $0^\circ$  and  $60^\circ$  wind incidence angle

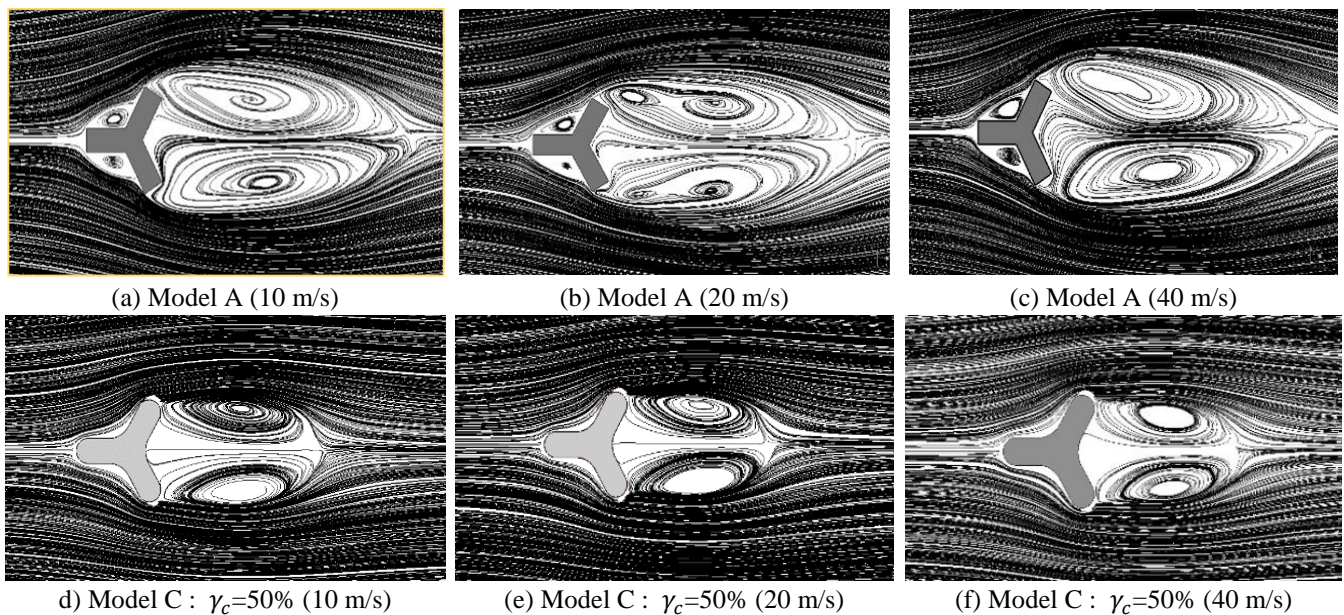


Fig. 30 Streamlines around model A and model C for different levels of wind velocity

29 also suggests that the aerodynamic behavior of Model A and E is almost same. Model C and D also follow the same wind pressure variation. So, we can conclude that the wind load reduction is mainly due to corner of the shorter edges. The corners at the intersection of the longer edges have almost negligible contribution in wind load reduction. But still this type of corners can be provided just to compensate the loss in plan area for shorter edge corner modifications and from aesthetic view point.

#### 4.6 Re number effect assessment

Different levels of wind-velocity were examined in order to analyze the effect of velocities and consequently different Reynolds number on the velocity profile and the force and moment coefficients. The examined velocities were as listed in Table 8. As shown in Fig. 30 the velocity profile and the wake size were very similar within the studied velocity range. The variation of force and moment coefficient did not exceed 6%. The results show a limited dependence of the air velocity on aerodynamic coefficients.

#### 4.7 Comparison of results for k-epsilon and SST turbulence model

Model A and Model C ( $\gamma_c=50\%$ ) are further analyzed to study the disparity in k-epsilon and SST turbulence models. For this reason, the force and moment coefficients and the local pressure variation along the horizontal centerlines are studied. The comparison of CF and CM are shown in Table 9. From the data it is quite clear that Model A shows almost similar data for both these turbulence models but for Model C these values are almost 10% less for SST model. The streamlines shown in Fig. 31 also justifies the drop in the wind force and moment. From the velocity contour it is quite clear that the wind velocity at the corner of the separation zone is higher for SST model and the wake size is also smaller. The pressure lines (Fig. 31) also suggests that for model A both these turbulence models show similar pressure variation but for Model C the separation corner zones have more suction for SST model

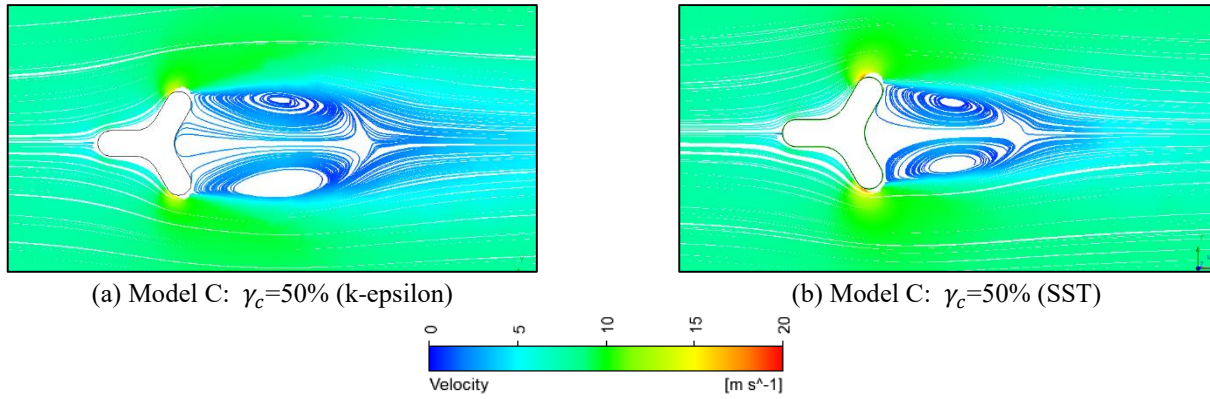


Fig. 31 Streamlines around Model C ( $\gamma_c=50\%$ ) for k-epsilon and SST turbulence models ( $AOA=0^\circ$ )

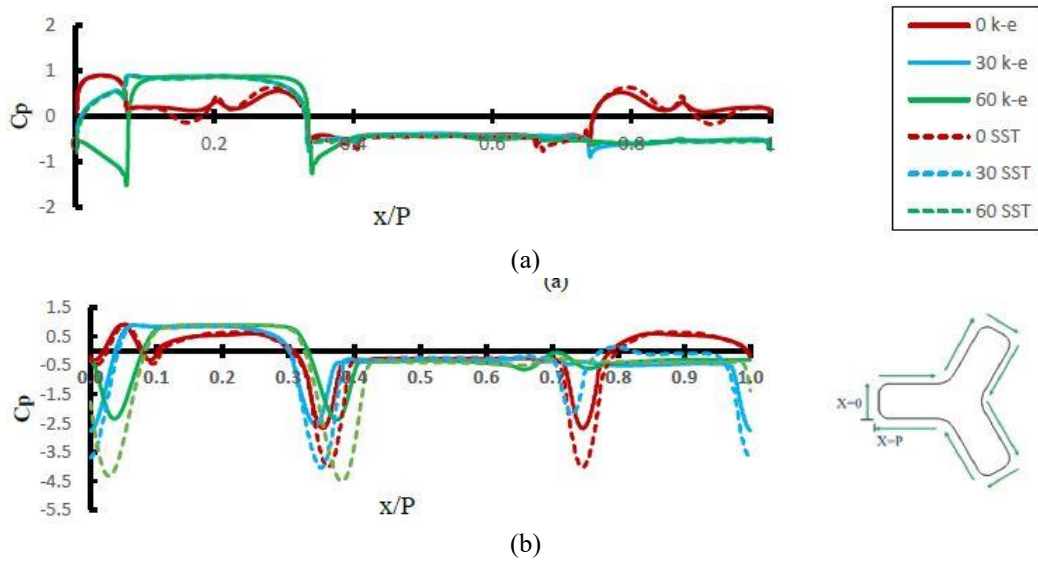


Fig. 32 Variation of pressure coefficients along perimeter of (a) Model A and (b) Model C ( $\gamma_c = 50\%$ ) for different AOA and turbulence model (at mid height)

Table 9 Comparison of Force and Moment Coefficients of Model A and C ( $\gamma_c = 50\%$ ), for k-epsilon and SST turbulence model

$\theta$	k-epsilon				SST			
	Model A		Model C ( $\gamma_c = 50\%$ )		Model A		Model C ( $\gamma_c = 50\%$ )	
	Force coefficient ( $C_F$ )	Moment coefficient ( $C_M$ )	Force coefficient ( $C_F$ )	Moment coefficient ( $C_M$ )	Force coefficient ( $C_F$ )	Moment coefficient ( $C_M$ )	Force coefficient ( $C_F$ )	Moment coefficient ( $C_M$ )
$0^\circ$	0.732	0.815	0.422	0.478	0.749	0.809	0.375	0.424
$30^\circ$	1.071	1.151	0.845	0.930	1.106	1.175	0.754	0.843
$60^\circ$	0.939	1.018	0.648	0.721	0.954	1.059	0.573	0.681

**5. Conclusions**

This paper described the effect of corner cut on wind load reduction of Y plan shaped tall building. CFD Simulation has been done by ANSYS CFX software. Wind tunnel results have been used to validate the k- $\epsilon$  and SST models. As k- $\epsilon$  models give almost similar results, it is used for the further numerical simulations. A comparison part for k- $\epsilon$  and SST turbulence model is also included at the end.

- The significant outcomes of the current study are
- In compare to chamfered corner, rounded corner is more efficient in reducing the wind load.
  - Within the studied wind angles the maximum force and moment coefficient is observed at 300 wind angle. By modifying the corner shapes, these maximum force and moment coefficient values could be lowered to up to 21.1 % and 19.2 % of that of the sharp edge model.
  - For designing of the corner modified Y plan shaped

buildings, the corner portions must be studied properly and special attention is required for cladding design.

- The reduction in wind load mainly occurs due to the corner of the shorter edges. The corners at the intersection of the longer edges have an almost negligible contribution in the wind load reduction.
- Dependency of aerodynamic coefficients on the air velocity and Reynold's Number is almost negligible.
- SST turbulence model predicts a higher reduction of wind force and moment coefficient for corner modified models and the suction is also higher in the separation corner zones.

## References

- Amano, T. (1995), "The Effect of corner-cutting of three dimensional square cylinders on vortex-induced oscillation and galloping in uniform flow", *J. Struct. Constr. Eng.*, AIJ 478, 63-69.
- Bairagi, A.K. and Dalui, S.K. (2015), "Comparison of aerodynamic coefficients of setback tall buildings due to wind load", *Asian J. Civil Eng.*, **19**(2), 205-221. <https://doi.org/10.1007/s42107-018-0018-3>.
- Baker, W.F., Korista, D.S. and Novak, L.C. (2007), "Burj Dubai: Engineering the world's tallest building", *Struct. Des. Tall Spec. Build.*, **16**(4), 361-375. <https://doi.org/10.1002/tal.418>.
- Bhattacharya, B. and Dalui, S.K. (2018), "Investigation of mean wind pressures on 'E' plan shaped tall building", *Wind Struct.*, **26**(2), 99-114. <https://doi.org/10.12989/was.2018.26.2.099>.
- Carassale, L., Freda, A. and Marrè-Brunenghi, M. (2014), "Experimental investigation on the aerodynamic behavior of square cylinders with rounded corners", *J. Fluids Struct.*, **44**, 195-204. <https://doi.org/10.1016/j.jfluidstructs.2013.10.010>.
- Celik, I.B., Ghia, U. and Roache, P.J. (2008), "Procedure for estimation and reporting of uncertainty due to discretization in CFD applications", *J. Fluids Eng.*
- Chakraborty, S., Dalui, S.K. and Ahuja, A.K. (2014), "Wind load on irregular plan shaped tall building - A case study", *Wind Struct.*, **19**(1), 59-73. <http://dx.doi.org/10.12989/was.2014.19.1.059>.
- Cheng, S.Y., Tsubokura, M., Nakashima, T., Nouzama, T. and Okada, Y. (2011), "A numerical analysis of transient flow past road vehicles subjected to pitching oscillation", *J. Wind Eng. Ind. Aerod.*, **99**(5), 511-522. <https://doi.org/10.1016/j.jweia.2011.02.001>.
- Cooper, K.R., Nakayama, M., Sasaki, Y., Fediw, A.A., Resende-Ide, S. and Zan, S.J. (1997), "Unsteady aerodynamic force measurements on a super-tall building with a tapered cross section", *J. Wind Eng. Ind. Aerod.*, **72**, 199-212. [https://doi.org/10.1016/S0167-6105\(97\)00258-4](https://doi.org/10.1016/S0167-6105(97)00258-4).
- Dalui, S.K. (2008), "Wind effects on tall buildings with peculiar shapes". Ph.D. Dissertation, Indian Institute of Technology Roorkee, India.
- Derakhshandeh, J.F. and Alam, M.M. (2018), "Flow structures around rectangular cylinder in the vicinity of a wall", *Wind Struct.*, **26**(5), 293-304.
- Elshaer, A., Bitsuamlak, G.T. and El Damatty, A. (2017), "Enhancing wind performance of tall buildings using corner aerodynamic optimization", *Eng. Struct.*, **136**, 133-148. <https://doi.org/10.1016/j.engstruct.2017.01.019>.
- Elshaer, A., Bitsuamlak, G.T. and El Damatty, A. (2014), "Vibration control of tall buildings using aerodynamic optimization", In: *25th CANCAM London*, Ontario, Canada.
- Elshaer, A., Bitsuamlak, G.T. and El Damatty, A. (2014), "Wind load reductions due to building corner modifications", In *22nd Annual Conference of the CFD Society of Canada*, Toronto, Canada.
- Elshaer, A., Bitsuamlak, G.T. and El Damatty, A. (2016), "Aerodynamic shape optimization of tall buildings using twisting and corner modifications", In: *8th International Colloquium on Bluff Body Aerodynamics and Applications Northeastern University*, Boston, U.S.A., June.
- Franke, J., Hirsch, C., Jensen, A.G., Krus, H.W., Schatzmann, M., Westbury P.S., Miles S.D., Wisse, J.A. and Wright, N.G. (2004), "Recommendations on the Use of CFD in Wind Engineering", *COST Action C14. European Science Foundation COST Office*.
- Fu, J.Y., Li, Q.S., Wu, J.R., Xiao, Y.Q. and Song, L.L. (2008), "Field measurements of boundary layer wind characteristics and wind induced responses of super-tall buildings", *J. Wind Eng. Ind. Aerod.*, **96**(8-9), 1332-1358. <https://doi.org/10.1016/j.jweia.2008.03.004>.
- Ghani, S. A., Aroussi, A. and Rice, E. (2001), "Simulation of road vehicle natural environment in a climatic wind tunnel", *Simul. Pract. Th.*, **8**(6-7), 359-375. [https://doi.org/10.1016/S0928-4869\(00\)00028-8](https://doi.org/10.1016/S0928-4869(00)00028-8).
- Gillieron, P. and Chometon, F. (2001), "Reduction of cooling air drag of road vehicle: an analytical approach", SAE 2001-01-1266. <https://doi.org/10.4271/2001-01-1266>.
- Gomes, M.G., Rodrigues, A.M. and Mendes, P. (2005), "Experimental and numerical study of wind pressures on irregular-plan shapes", *J. Wind Eng. Ind. Aerod.*, **93**(10), 741-756.
- Gu, M. and Quan, Y. (2004), "Across-wind loads of typical tall buildings", *J. Wind Eng. Ind. Aerod.*, **92**(13), 1147-1165. <https://doi.org/10.1016/j.jweia.2004.06.004>.
- Irwin, P.A. (2009), "Wind engineering challenges of the new generation of super-tall buildings", *J. Wind Eng. Ind. Aerod.*, **97**(7-8), 328-334. <https://doi.org/10.1016/j.jweia.2009.05.001>.
- Jacobsen, M. (2006), "Real time drag minimization using redundant control surfaces", *Aerosp. Sci. Technol.*, **10**(7), 574-580. <https://doi.org/10.1016/j.ast.2006.05.002>.
- Jones, W.P., and Launder, B.E. (1972), "The prediction of laminarization with a two-equation model of turbulence", *Int. J. Heat Mass Trans.*, **15**(2), 301-314.
- Kawai, H. (1998), "Effects of corner modifications on aeroelastic instabilities of tall buildings", *J. Wind Eng. Ind. Aerod.*, **74**, 719-729. [https://doi.org/10.1016/S0167-6105\(98\)00065-8](https://doi.org/10.1016/S0167-6105(98)00065-8).
- Kim, Y.C. and Kanda, J. (2010a), "Characteristics of aerodynamic forces and pressures on square plan buildings with height variations", *J. Wind Eng. Ind. Aerod.*, **98**(8-9), 449-465. <https://doi.org/10.1016/j.jweia.2010.02.004>.
- Kim, Y.C. Kanda, J. (2010b), "Effects of taper and set-back on wind force and wind-induced response of tall buildings", *Wind Struct.*, **13**(6), 499-517. <https://doi.org/10.12989/was.2010.13.6.499>.
- Kim, Y.M. and You, K.P. (2002), "Dynamic responses of a tapered tall building to wind load", *J. Wind Eng. Ind. Aerod.*, **90**(12-15), 1771-1782. [https://doi.org/10.1016/S0167-6105\(02\)00286-6](https://doi.org/10.1016/S0167-6105(02)00286-6).
- Kim, Y.M., You, K.P. and Ko, N.H. (2008), "Across-wind response of an aeroelastic tapered tall building", *J. Wind Eng. Ind. Aerod.*, **96**(8-9), 1307-1319.
- Kumar, D. and Dalui, S.K. (2017), "Effect of internal angles between limbs of cross plan shaped tall building under wind load", *Wind Struct.*, **24**(2), 95-118. <https://doi.org/10.12989/was.2017.24.2.095>.
- Kumar, E.K., Tamura, Y., Yoshida, A., Kim Y.C. and Yang, Q. (2013), "Journal of wind engineering experimental investigation on aerodynamic characteristics of various triangular-section high-rise buildings", *J. Wind Eng. Ind. Aerod.*, **122**, 60-68.
- Kwok, K.C.S. and Bailey, P.A. (1987), "Aerodynamic devices for tall building and structures", *J. Eng. Mech.* **113**(3), 349-365.

- [https://doi.org/10.1061/\(ASCE\)0733-9399\(1987\)113:3\(349\)](https://doi.org/10.1061/(ASCE)0733-9399(1987)113:3(349)).
- Kwok, K.C.S., Wilhelm, P.A. and Wilkie, B.G. (1988), "Effect of edge configuration on wind-induced response of tall buildings", *Eng. Struct.*, **10**(2), 135-140. [https://doi.org/10.1016/0141-0296\(88\)90039-9](https://doi.org/10.1016/0141-0296(88)90039-9).
- Miyashita, K., Katagiri, J., Nakamura, O., Ohkuma, T., Tamura, Y., Itoh, M. and Mimachi, T. (1993), "Wind-induced response of high-rise buildings effects of corner cuts or openings in square buildings". *J. Wind Eng. Ind. Aerod.*, **50**, 319-328. [https://doi.org/10.1016/0167-6105\(93\)90087-5](https://doi.org/10.1016/0167-6105(93)90087-5).
- Modi, V.J., Hill, S.S.T. and Yokomizo, T. (1995), "Drag reduction of trucks through boundary-layer control", *J. Wind Eng. Ind. Aerod.*, **54**, 583-594. [https://doi.org/10.1016/0167-6105\(94\)00074-N](https://doi.org/10.1016/0167-6105(94)00074-N).
- Mohamed-Kassim, Z. and Filippone, A. (2010), "Fuel savings on a heavy vehicle via aerodynamic drag reduction", *Transportation Research Part D: Transport. Environ.*, **15**(5), 275-284. <https://doi.org/10.1016/j.trd.2010.02.010>.
- Muehleisen, R.T. and Patrizi, S. (2013), "A new parametric equation for the wind pressure coefficient for low-rise buildings", *Energy and Build.*, **57**, 245-249. <https://doi.org/10.1016/j.enbuild.2012.10.051>.
- Mukherjee, S., Chakraborty, S., Dalui, S.K. and Ahuja, A.K. (2014), "Wind-induced pressure on "Y" plan shape tall building", *Wind Struct.*, **19**(5), 523-540. <https://doi.org/10.12989/was.2014.19.5.523>.
- Raj, R. and Ahuja, A.K. (2013), "Wind loads on cross shape tall buildings", *J. Acad. Ind. Res.*, **2**(2), 111-113.
- Sanyal, P. and Dalui, S.K. (2018), "Effects of courtyard and opening on a rectangular plan shaped tall building under wind load", *Int. J. Adv. Struct. Eng.*, **10**(2), 169-188. <https://doi.org/10.1007/s40091-018-0190-4>.
- Shiraishi, N., Matsumoto, M., Shirato, H., Ishizaki, H., Osada, M. and Matsui, T. (1986), "On aerodynamic stability effects for bluff rectangular cylinders by their corners cut", *J. Wind Eng. Ind. Aerod.*, **28**(1-3), 371-380.
- Song, J., Tse, K.T., Tamura, Y. and Kareem, A. (2016), "Aerodynamics of closely spaced buildings: with application to linked buildings", *J. Wind Eng. Ind. Aerod.*, **149**, 1-16.
- Sun, X., Liu, H., Su, N. and Wu, Y. (2017), "Investigation on wind tunnel tests of the kilometer skyscraper", *Eng. Struct.*, **148**, 340-356. <https://doi.org/10.1016/j.engstruct.2017.06.052>.
- Tamura, T. and Miyagi, T. (1999) "The effect of turbulence on aerodynamic forces on a square cylinder with various corner shapes", *J. Wind Eng. Ind. Aerod.*, **83**(1-3), 135-145. [https://doi.org/10.1016/S0167-6105\(99\)00067-7](https://doi.org/10.1016/S0167-6105(99)00067-7).
- Tamura, T., Miyagi, T. and Kitagishi, T. (1998), "Numerical prediction of unsteady pressures on a square cylinder with various corner shapes", *J. Wind Eng. Ind. Aerod.*, **74**, 531-542.
- Tanaka, H., Tamura, Y., Ohtake, K., Nakai, M. and Chul Kim, Y. (2012), "Experimental investigation of aerodynamic forces and wind pressures acting on tall buildings with various unconventional configurations", *J. Wind Eng. Ind. Aerod.*, **107**, 179-191.
- Tse, K.T., Hitchcock, P.A., Kwok, K.C.S., Thepmongkorn, S. and Chan, C.M. (2009), "Economic perspectives of aerodynamic treatments of square tall buildings", *J. Wind Eng. Ind. Aerod.*, **97**(9-10), 455-467. <https://doi.org/10.1016/j.jweia.2009.07.005>.
- Watkins, S., Saunders, J.W. and Hoffmann, P.H. (1993), "Comparison of road and wind tunnel drag reductions for commercial vehicles", *J. Wind Eng. Ind. Aerod.*, **49**(1-3), 411-420.
- Yi, J. and Li, Q.S. (2015), "Wind tunnel and full-scale study of wind effects on a super-tall building", *J. Fluids Struct.*, **58**, 236-253.
- Zhengwei, Z., Yonga, Q., Minga, G., Nankuna, T. and Yongc, X., (2012), "Effects of corner recession modification on aerodynamic coefficients of square tall buildings", *In the Seventh International Colloquium on Bluff Body Aerodynamics and Applications*, China, September.

AD